DYNAMIC MODELING AND CONTROL SYSTEM FOR A SHROUDED PROPELLER SYSTEM

Y.D. Jung *, G.H. Kim **, D.H. Shim*, S.O. Park******
***KAIST, Daejeon 305-701, Republic of Korea**

Keywords: *shrouded propeller system, UAV, dynamic modeling, classical control*

Abstract

This paper is presents the dynamic modeling and control system design of a shrouded propeller based on the classical method. The dynamic model has been designed using nonlinear aerodynamic models by VLM (Vortex Lattex Method). The aerodynamic analysis of the model is indispensible for the improvement of its accuracy and for designing the controller. Based on the LTI model of hover, classical SISO control has been used for the stabilization of the vehicle. The controller for hover has been designed using the linear SISO control approach. Further, the control system design has been based on the precise dynamic model for more accurate controller gain selection. The proposed controllers have been presented along with the simulation results. In conclusion, the performance of the proposed approach has first been validated by numerical simulation and then by a series of flight tests.

1. Introduction

There has recently been increased emphasis on the use of UAVs (unmanned aerial vehicles) in various activities for both civilian and military applications. Such applications include surveillance, reconnaissance, target tracking, data acquisition, jamming, communications relay, decoy, or harassment [1]. Fixed-wing UAVs are predominantly employed due to low cost, high efficiency and speed, and long operation range. However, much of their operational flexibility is lost if runways are not available for take-offs and landings. On the contrary, VTOL UAVs can be operated even in the absence of a runway and are suitable for various applications, especially in urban environments having a few obstacles. Rotorcraft-based UAVs are desirable for certain applications where the unique flight capability of a rotorcraft is required. The rotorcraft is useful for applications, such as, low-speed tracking maneuvers, reconnaissance, and operations where no runway is available for take-off and landing.

Considerable research has been carried out on the development of autonomous helicopters due to their high availability. However, it is dangerous to operate helicopters in cluttered environments due to their exposed rotor blades. The shrouded fan VTOL UAV was conceptualized in order to ensure protection from the exposed helicopter rotor blades. Thus, the protected propeller would be able to execute the mission even in the presence of obstacles and people

The presence of momentum drag, an aerodynamic parameter that yields a significant pitching moment, lends the shrouded propeller concept its novelty. However, this moment also makes the vehicle very unstable such that even an experienced pilot would not be able to keep it steady during flight without an active controller.

A reasonably accurate model is helpful for simulation, especially during the early phases of design and flight testing. An accurate simulator allows designers to estimate the performance of the controllers. The performance of the controller during various maneuvers can also be evaluated in order to reduce the risks during flight tests. A simulation model of the shrouded propeller system was developed using analysis and experimentation.

This paper presents the dynamic modeling and control system design of a shrouded propeller

system based on the classical method. The dynamic model of a shrouded propeller was developed using nonlinear aerodynamic models with the help of VLM. Dynamic equations having 6 degrees of freedom (DOF), which also include aerodynamic characteristics, have been derived. Aerodynamic analysis is indispensible for the improvement of accuracy of the model in order to design the controller. Based on the LTI model of hover, classical SISO control is used for vehicle stabilization. Further, by using a control system design based on the precise dynamic model, more accurate controller gain selection is possible. The proposed controllers have been presented along with the simulation results. Finally, the performance of the proposed approach is first validated using numerical simulation and then a series of flight tests.

2. System Configuration

One of the main goals of this research is to develop and establish a comprehensive and practical methodology in order to design and implement a shrouded propeller UAV equipped with a reliable and highly accurate autopilot. In order to achieve this goal, we need to integrate the vehicle platform with appropriate hardware and software so that the vehicle performs the desired autonomous maneuvers. In this section, we have presented details of the airframe, hardware, and software of the shrouded propeller.

2.1 Airframe and avionics

It is possible to control the attitude of the aircraft having the designed shrouded propeller even in crosswind. Therefore, the basic configuration of a shrouded propeller has control vanes mounted under the shroud for control [2].

This configuration has several benefits as compared to general UAV configurations. Firstly, the shroud system, which envelops the propeller and engine, reduces propeller hazards and increases the static thrust. Secondly, control vanes are used to stabilize the UAV throughout the entire flight envelope. The vanes attached below the slipstream of the propeller always produce control moment regardless of the flight condition.

Fig.1 shows the configuration of the designed shrouded propeller UAV. The designed shrouded propeller UAV has a nominal gross weight of 9.5 kg and shroud diameter 0.66 m. The platform is powered by Lithium-polymer cells and a brushless DC motor.

Fig. 1. Shrouded Propeller

The avionics suite consists of a flight control computer (FCC), inertial measurement unit (IMU), GPS sensor, and servo controller module, as shown in Fig. 2. The flight control computer is constructed using PC104-compatible boards due to their industry-grade reliability, compactness, and expandability. The navigation system is built using GPS-aided INS. NovAtel OEM-V2-RT2 is used due to its excellent tracking capability as well as high accuracy. 3DM-GX IMU has low weight and shows good performance during flight. The vehicle communicates with the ground station through a high-bandwidth telemetry link at 900 MHz to reduce communication latency. The acceleration and angular rate of the vehicle are read in flight computer via serial ports, and are used in the navigational routine, which is processed at 100 Hz, for the calculation of position, attitude, and, heading. The inertial measurement sensor error is estimated and compensated using the Extended Kalman Filter (EKF), processing at 5 Hz, while the GPS calculates its position. The detailed specifications are listed in Tab. 1.

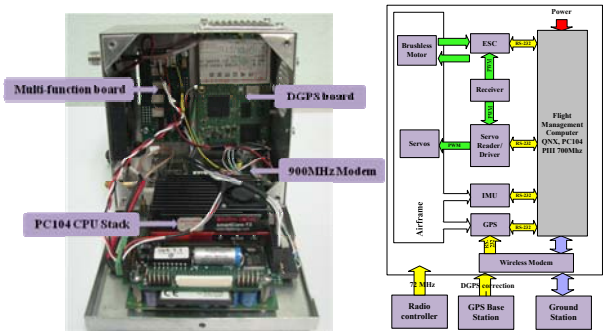

Fig. 2. Flight Computer based on PC104

Tab. 1. Specification of Designed Shrouded Propeller

Dimensions	Height : 0.89 m Shroud Diameter : 0.66 m
Weight	9.5 kg (fully instrumented)
Power plant	Plettenberg DC Brushless Motor 26 × 8 propeller Lithium-Ion-Polymer
Avionics	Differential GPS-aided INS GPS: NovAtel OEM-V2-RT2 IMU: 3DM-GX3 Flight Computer: PC104 Communication: 900MHz

2.2 Control Surfaces of a shrouded propeller UAV

The control surfaces of a shrouded propeller UAV are different from general UAVs. The vanes attached under the slipstream of the propeller always produce control moment regardless of the flight condition.

The vane system has four control surfaces, each operating independently. Control inputs consist of roll, pitch, and yaw given by:

$$\begin{aligned} \delta_{ele} &= \delta_{left} + \delta_{right} \\ \delta_{ail} &= \delta_{down} - \delta_{left} + \delta_{right} - \delta_{up} \\ \delta_{rdr} &= \delta_{up} + \delta_{down} \end{aligned} \qquad (1)$$

where δ is the deflection angle of the vanes and the subscripts (left, right, down, and up) indicate the position of the vanes. The motion of the vanes is similar to the ailerons when the symmetrically positioned vanes move in opposite directions, and it is similar to the elevator and rudder when they move together in the same direction.

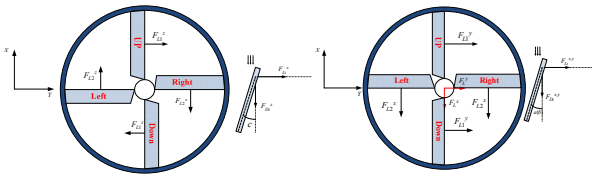

Fig. 3. Vane System

3. Dynamic Modeling

3.1 Equation of Motion

The initial stage of the autonomous flight control system is a full nonlinear 6-DOF model of the shrouded propeller UAV. The 6-DOF rigid-body equations of motions are expressed as the following set of differential equations [3]:

$$m\dot{\mathbf{v}}_B + \boldsymbol{\omega} \times m\mathbf{v}_B = \mathbf{F}_B + m\mathbf{g} + \mathbf{F}_\mathbf{u} \qquad (2)$$

$$\mathbf{I}\dot{\boldsymbol{\omega}} = -\boldsymbol{\omega} \times \mathbf{I}\boldsymbol{\omega} + \mathbf{M}_B + \mathbf{M}_\mathbf{u} \qquad (3)$$

where

$$\mathbf{v}_B = \begin{bmatrix} u & v & w \end{bmatrix}^T$$

u, v, and w are the longitudinal, lateral, and vertical body velocities, respectively, and

$$\boldsymbol{\omega} = \begin{bmatrix} p & q & r \end{bmatrix}^T$$

p, q, and r are the roll, pitch, and yaw body rates, respectively, and $\mathbf{I}$ is the inertia matrix. . $\mathbf{F_u}$ and $\mathbf{M_u}$ represent control force and moment by control vane, respectively. $\mathbf{F_B}$ and $\mathbf{M_B}$ are the vectors used to denote the external force and moment components, respectively, with respect to the body-fixed frame. These external forces and moments can be expressed as follows [4]:

$$\begin{aligned} \mathbf{F}_B &= \mathbf{F}_{aero} + \mathbf{F}_{propeller} + \mathbf{F}_{mdrag} \\ \mathbf{M}_B &= \mathbf{M}_{aero} + \mathbf{M}_{propeller} + \mathbf{M}_{gyro} + \mathbf{M}_{mdrag} \end{aligned} \qquad (4)$$

The subscript $()_{aero}$ indicates the effect of aerodynamic forces and moments. $()_{propeller}$ indicates the effect of shrouded propeller. Further, $()_{mdrag}$ indicates the effect of the momentum drag, $()_{gyro}$ indicates the gyro effects

of the propeller. The gyroscopic moments $\mathbf{M}_{gyro}$ induced due to the gyroscopic effect can be given by:

$$\mathbf{M}_{gyro} = -b_i i_b \omega_r \begin{bmatrix} -\omega_y \\ \omega_x \\ 0 \end{bmatrix} \quad (5)$$

3.2 Aero data

Aerodynamic forces $\mathbf{F}_{aero}$ and moments $\mathbf{M}_{aero}$ due to the fuselage, wing, and shroud can be written as:

$$\mathbf{F}_{aero} = \begin{bmatrix} -q_\infty S C_{D_x}^{\ Total} \\ q_\infty S C_{D_y}^{\ Total} \\ -q_\infty S C_L^{\ Total} \end{bmatrix} \quad (6)$$

$$\mathbf{M}_{aero} = \begin{bmatrix} q_\infty S c C_{M_x}^{\ Total} \\ q_\infty S c C_{M_y}^{\ Total} \\ 0 \end{bmatrix} \quad (7)$$

where q_∞ is dynamic pressure, S is the shroud area and c is the length of shroud. It is note that aerodynamic coefficients are calculated about each direction of these coefficients using C_L, C_D, and C_M

Aerodynamic coefficients have been analyzed using the empirical formula and the Vortex Lattice Method [2]. When VLM is for aerodynamic analysis, the shroud is modeled to be polygonal. The non-dimensional stability derivatives obtained from the aerodynamic model and VLM are functions of the angle of attack and Mach number. For calculation of coefficients, the AVL code developed at MIT has been used by making some modifications for the present application. The aero data is used by look up table. The angle of attack ranges from -10° to 12° and Mach number from 0 to 0.1. In order to increase the angle of attack range to include possible higher angles of attack at hover due to crosswind, the calculated aerodynamic model is extrapolated using the aerodynamic characteristics of NACA 0012 airfoil.

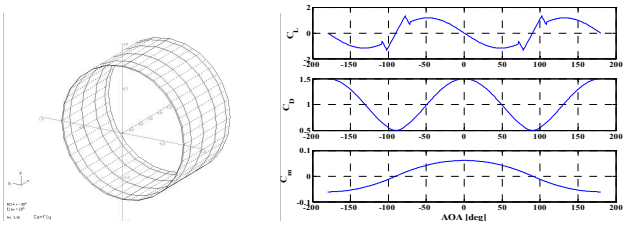

Fig. 4. Aerodynamic Analysis of a shroud

The thrust $\mathbf{F}_{\text{propeller}}$ and anti-torque generated by the revolution of propeller $\mathbf{M}_{\text{propeller}}$ can be given as follows:

$$\mathbf{F}_{propeller} = \begin{bmatrix} 0 \\ 0 \\ -T \end{bmatrix} \quad (8)$$

$$\mathbf{M}_{propeller} = \begin{bmatrix} 0 \\ 0 \\ -M_e \end{bmatrix} \quad (9)$$

where M_e is the propeller power and T is thrust. In order to show effect of the shrouded propeller, Ducted Fan Design Code (DFDC) is used since the shroud improves the static thrust of the shrouded propeller as compared to the thrust of an open propeller of the same diameter [5].

$\mathbf{F}_{mrag}$ and $\mathbf{M}_{mdrag}$ are the vectors used to represent the forces and moments, respectively, created due to momentum drag, which is generated by changing the incoming flow direction and making it downward. The centre of pressure of the momentum drag is at the upper center of gravity (CG) which is shroud. Therefore, the momentum drag acts at the centre of pressure (CP) and produces moment about the centre of gravity. The centre of pressure may be located at the lip of the shroud. These external forces and moments can be expressed as [2]:

$$\mathbf{F}_{mdrag} = -\dot{m} \begin{bmatrix} 0 \\ v_y \\ v_z \end{bmatrix} \quad (10)$$

$$\mathbf{M}_{mdrag} = -\dot{m} l_{lip} \begin{bmatrix} 0 \\ v_y \\ v_z \end{bmatrix} \quad (11)$$

where v_y and v_z are the crosswind velocity components at the shroud. These velocities are not equal to the crosswind velocity acting on the aircraft. l_{lip} is the distance of the shrouded propeller CG from the shroud lip, $\dot{m}$ is mass flow rate.

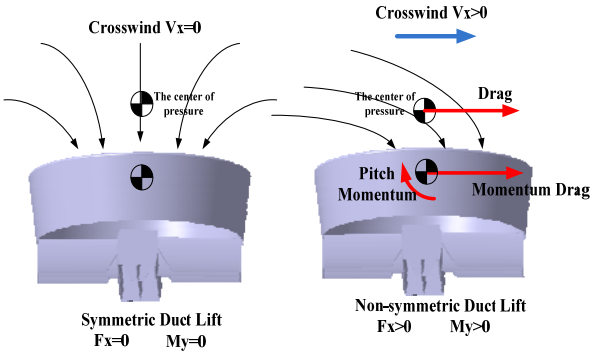

Fig. 5. Effects of a Shroud with Crosswind

Control force $\mathbf{F_u}$ and moment $\mathbf{M_u}$ acting on the tail-sitter UAV induced by the control surfaces can be written as [5]:

$$\mathbf{F_u} = q_v S_v \begin{bmatrix} -C_{F_v}\delta_{ele} \\ -C_{F_v}\delta_{ail} \\ 0 \end{bmatrix} \tag{12}$$

$$\mathbf{M}_u = q_v S_v \begin{bmatrix} l_v C_{F_v}\delta_{ail} \\ l_v C_{F_v}\delta_{ele} \\ 2d_v C_{F_v}\delta_{rud} \end{bmatrix} \tag{13}$$

where l_v is the distance between the CG of the vehicle and 1/4th chord of the vanes, d_v is the distance between the central axis and the vanes, and q_v is dynamic pressure in the duct.

Aerodynamic control coefficient C_F is obtained using VLM method from the aerodynamic model described earlier. Force coefficient of the control vanes is analyzed using the Navier-Stokes solver FLUENT by momentum source method for rotor disc simulation and compared with the experiment results for verification of the calculations.

In the experiment, the control forces are measured from the test-bed designed, as shown in Fig. 6. This test-bed is connected at the estimated CG of the tail-sitter by means of a ball joint to rotate only in one direction. The vanes are deflected at constant propeller speed then the inclined angle of the shroud is measured for the calculation of control forces. This measurement is a function of the deflection angle and propeller rpm. Therefore, the experiment is conducted from 2500 to 4000 rpm and from 0 to 20° vane deflection.

The numerical results and experiment data are shown in Fig. 7. Note that the VLM results showed a noticeable deviation from the experimental data points. On the other hand, the numerical results obtained using FLUENT seemed to be well in agreement with the experimental data points. Further, note that the thrust of the shrouded propeller is calculated using Blade Element Method (BEM), and this result is reflected in the propeller disc of FLUENT.

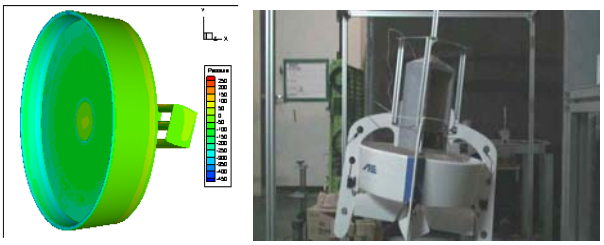

Fig. 6. Vane System of FLUENT and Experiment

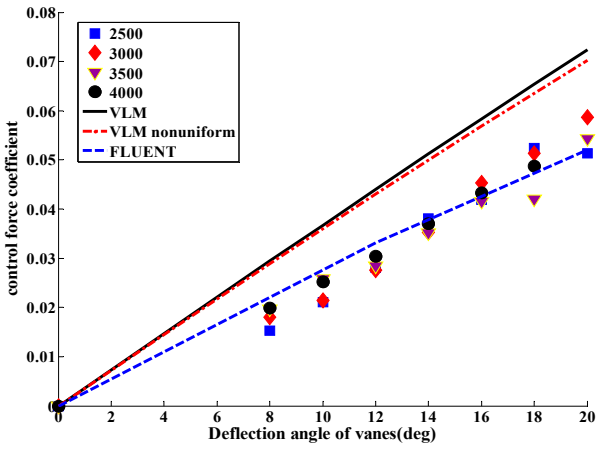

Fig. 7. Comparison of Numerical and Experimental Results

3.3 Actuator and Vane deflection angle

Servo motors are the most common type of actuators used on small UAVs. A shrouded propeller UAV uses four servo motors to control the vanes. The servo motor is controlled by a

PWM (pulse-width modulation) signal. The relation between vane angle and PWM should be analyzed since control inputs at modeling carried out at previous chapters are the deflection angle of vanes.

In order to obtain the relation between the vane deflection angle and PWM, the deflection angle is measured using an inclinometer while PWM is constantly generated. Measurements are linear from -40 to 40°. The simulation results can be applied to the flight test due to this linear relation. Therefore, this measurement can improve the accuracy of modeling.

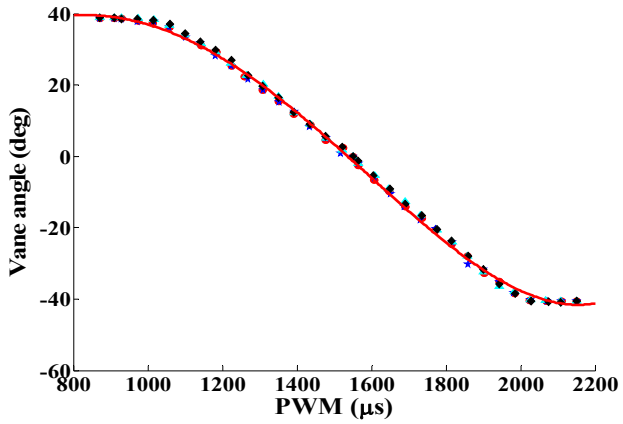

Fig. 8. Relation between PWM and Vane Angle

4. Control System Design

Our goal in this research is to provide a working autopilot system for our UAV. Therefore, we choose to deploy linear control theory for its consistent performance, well-defined theoretical background and effectiveness proven by many practitioners. Since the classical control approach is applicable to the SISO system, the MIMO UAV dynamics can be decoupled into SISO sub-systems. The system can be considered to be made up of four sub-systems that consist of roll, pitch, yaw and heave channels, and each can be stabilized by a proportional-differential (PD) controller. The roll and pitch dynamics are similar to each other due to symmetry of the geometrical characteristics.

The control law of the classical SISO approach is established as shown in Fig 9. Currently, it does not involve any dynamic controllers yet the static control achieves a reasonably good performance which can be written as [6]:

$$\begin{aligned}
\delta_{ail} &= -K_{\phi}\phi - K_{p}p - K_{v}v - K_{Y}\Delta_{Y} \\
\delta_{ele} &= -K_{\theta}\theta - K_{q}q - K_{u}u - K_{X}\Delta_{X} \\
\delta_{rud} &= -K_{\psi}\Delta_{\psi} - K_{r}r \\
\delta_{th} &= -K_{w}w - K_{Z}\Delta_{Z}
\end{aligned} \tag{14}$$

where K_{φ}, K_{θ}, and K_{ψ} are the feedback gains for roll, pitch, and yaw angles, K_u, K_v, and K_w represent feedback gains for u and v velocities. Further, K_X, K_Y, and K_Z are feedback gains for position and Δ denotes the difference between the desired and current values. The control system of our shrouded propeller system consists of attitude, velocity, and position controller. The attitude and velocity controller can stabilize unstable dynamic. The position controller can track desired position to selected waypoint.

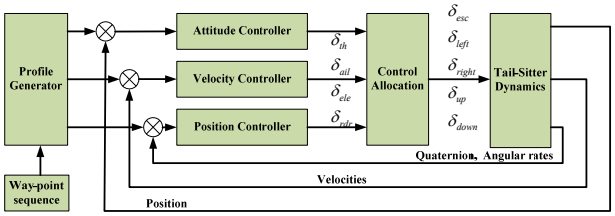

Fig. 9. Architecture of SISO Multi-loop Controllers

The attitude dynamics of the UAV in hover is similar to the inverted pendulum and clearly unstable. Therefore, the eigenvalues of the attitude dynamics of a tail-sitter are 0.8, and they can be stabilized by giving proportional feedback of each attitude angle and angular rate. Once the roll and pitch sub-dynamics are stabilized, we proceed to find the stabilizing feedback gains for the velocity and position dynamics using SISO root locus method and nonlinear simulation. We can proceed in a similar way to design the compensators for heave and yaw dynamics. Heave dynamics is inherently stable due to the aerodynamic effects of the propeller. However, velocity feedback can improve the damping of heave dynamics. Altitude control can be realized using proportional altitude error feedback.

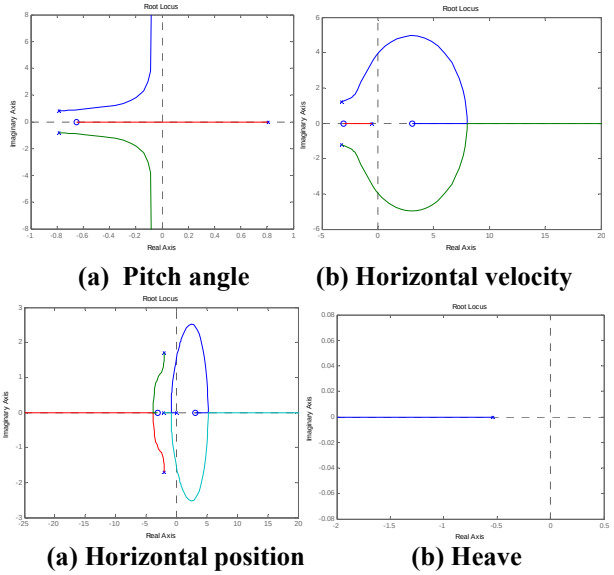

(a) Pitch angle (b) Horizontal velocity

(a) Horizontal position (b) Heave

Fig. 10. SISO Root Locus

5. Simulation Results

Simulation indicating the performance to be expected of the control system is provided using a waypoint guidance law. In the waypoint flight envelope, the vehicle turns to the target waypoint then goes through acceleration, cruise, and deceleration phases. The heading is constantly controlled during the whole time in order to point the target waypoint. The waypoint navigator generates the reference values for velocity, position, and heading and passes them to the low-level controller in real-time. The vehicle maintains a constant ground speed and the heading remains fixed. Therefore, the waypoint navigator must generate the reference position commands.

A simulation was set up where the tail-sitter UAV begins at the origin with zero heading angle. The cruise velocity is 1 m/s and error bond is 0.5 m for change of target waypoint. The waypoints were commanded in the following sequence:

- The aircraft is commanded 10 m north then heading is 90°
- The aircraft is commanded 10 m east then heading is 180°
- The aircraft is commanded 0 m north then heading is 270°
- The aircraft is commanded to origin point with zero heading

Figures 11 – 13 present the position, attitude, and control input states of the UAV during the maneuvers. As shown, when the UAV enters the neighborhood of a waypoint, it changes the heading and leaves for the next waypoint. It is evident from the figure that the aircraft successfully tracks the desired waypoints with just a small deviation. Results of the simulation indicate that simple SISO control of the hover mode can be carried out with adequate accuracy.

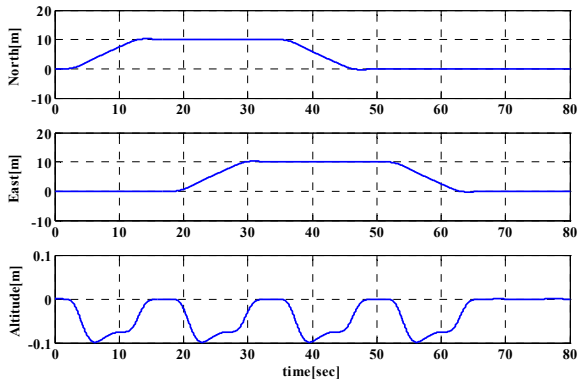

Fig. 11 Simulation Result of Position-time History

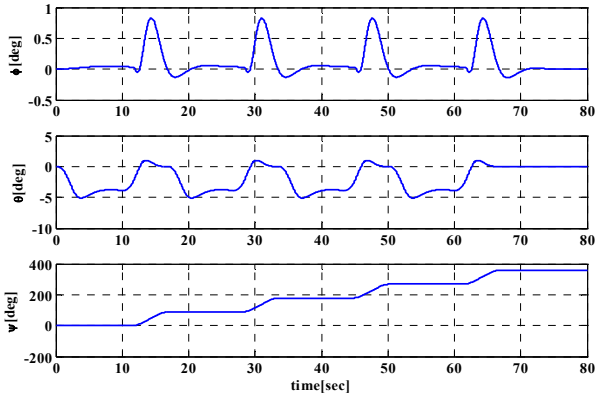

Fig. 12. Simulation Result of Attitude-time History

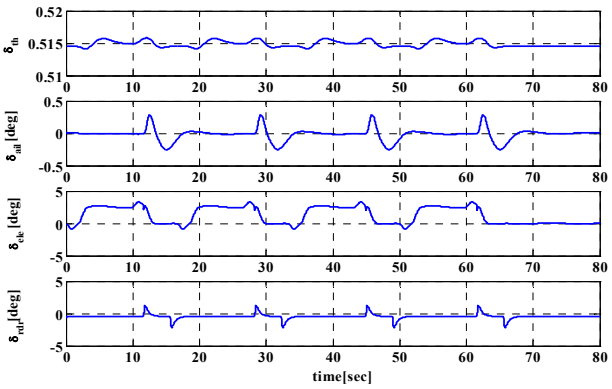

Fig. 13. Simulation Result of Control Input History

6. Flight Test

The autopilot system is demonstrated using the flight test results and the dynamic model is verified by comparing controller gains of nonlinear simulation and the flight test. In order to verify the performance of the controllers and the accuracy of dynamic model, the flight test is performed using the shrouded propeller system.

Fig. 14. Flight Test of a Shrouded Propeller

In this experiment, the take-off and landing is achieved using the designed compensators since such systems are known to be too unstable to be handled by a human pilot without controllers.

Using the attitude controller, we conducted a fully autonomous flight using waypoint guidance law. The vehicle passed by the target waypoints, which appeared to be like squares, and returned the start position. Figures 15–17 show the position, velocity, attitude, and control input response during the fully autonomous flight of the UAV. The shrouded propeller system showed a stable and sufficiently accurate response in attitude, velocity, and position. Positions show outstanding performance with ±0.5 m error. A series of experiments have been performed using the proposed controller to demonstrate the validity of the theoretical results.

The dynamic model has not been directly verified. However, we can verify the dynamic model indirectly by comparing the controller gains used during flight with those designed in the simulations. Tab. 2 shows the controller gains of flight test and nonlinear simulation.

The gains of roll and pitch rate feedback are limited due to signal noise of the IMU sensor. Therefore, there are oscillations in the control surfaces due to the noise of the angular rate. Accordingly, the values of K_p, K_q, and K_r are reduced during the experiments. Consequently, the dynamic model has accuracy for using the design of controllers since the controller gains selected by nonlinear simulations and experiments are very similar.

Tab. 2. Comparison Gains between Simulation and Flight Test

Nonlinear Simulation	Flight Test
$K_p = K_q = 0.9$	$K_p = K_q = 0.5$
$K_\phi = K_\theta = 2.0$	$K_\phi = K_\theta = 2.0$
$K_r = 0.4, K_\psi = 1.0$	$K_r = 0.3, K_\psi = 0.7$
$K_u = K_v = 0.15$	$K_u = K_v = 0.4$
$K_X = K_Y = 0.15$	$K_X = K_Y = 0.4$
$K_w = 0.1, K_Z = 0.07$	$K_w = 0.1,\ K_Z = 0.07$

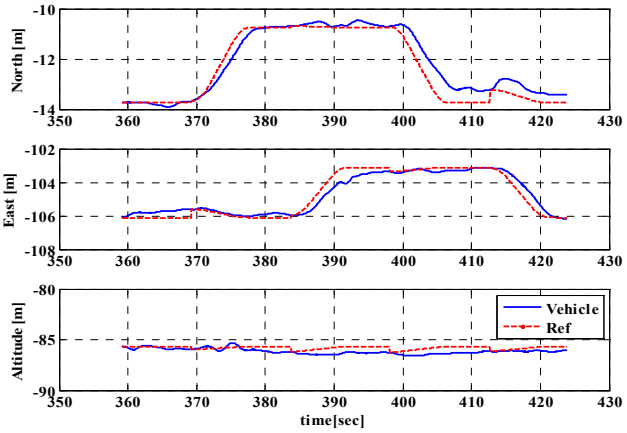

Fig. 15. Flight Test Result of Position

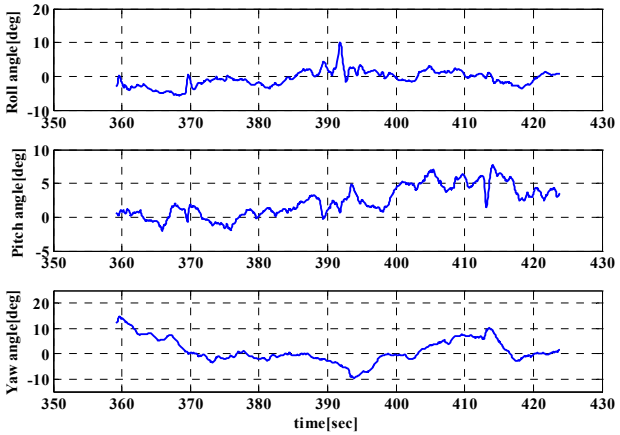

Fig.16. Flight Test Result of Attitude

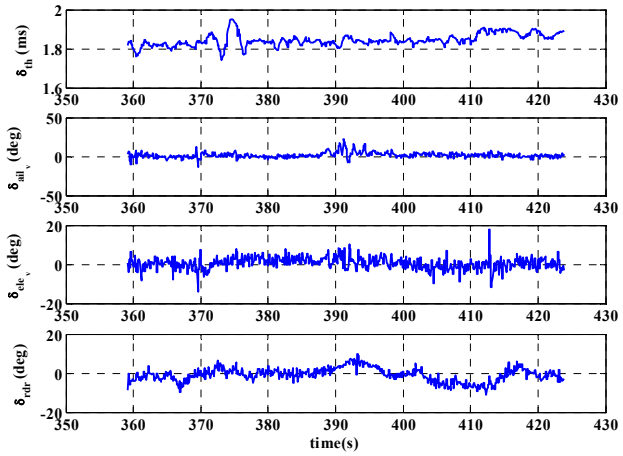

Fig. 17. Flight Test Result of Control Input

7. Conclusion

In this paper, we have presented the development of a practical flight control system and the dynamic modeling of a shrouded propeller system. The dynamic model of a shrouded propeller was designed using nonlinear aerodynamic models. Dynamic equations, which include aerodynamic characteristics, have been derived. The system has been analyzed with respect to the aerodynamic characteristics, which helps in understanding its dynamic properties.

Based on the LTI model of hover and horizontal flight, classical SISO control has been employed for vehicle stabilization. Further, the control system design is based on the precise dynamic model in order to make achieve highly accurate controller gain selection. The SISO multi-loop controller has then been used as a low-level vehicle stabilizer, and it has been integrated with the middle level waypoint navigator. The waypoint navigator generates reference positions and heading angles. Finally, the performance of the proposed approach has first been validated by numerical simulation and then by a series of flight tests. In similar experiments, the designed shrouded propeller showed good controller performance and the dynamic model was verified.

Acknowledgments

Authors are gratefully acknowledging the financial support by Agency for Defense Development and by UTRC (Unmanned Technology Research Center) and Brain Korea 21 Project, Korea Advanced Institute of Science and Technology.

Copyright Statement

References

[1] Unmanned Systems Roadmap 2007-2032, Department of Defense, U.S.A (2007)

[2] Y.Jeong, G.Kim, D.H.Shim, S.Park, Configuration Design and Modeling of a Tail Sitter VTOL UAV, *The KSAS 2009 Spring Conference* , Pyeongchang, 2009

[3] B. L. Stevens and F. L. Lewis, *Aircraft control and simulation*, John Wiley & Sons, INC, 1992.

[4] Eric N. Johnson and Michael A. Turbe, Modeling, Control, and Flight Testing of a Small Ducted Fan Aircraft, *AiAA Guidance, Navigation, and Control Conference and Exhibit*, 15 – 18, 2005

[5] G.Kim , Y.Jeong, D.H.Shim, S.Park, Measurement and Prediction of Control Vane Force in the Wake of a shrouded Propeller, *The KSAS 2009 Fall Conference* , Gyeongju, 2009

[6] M. Drela, H. Youngren, "Axisymmetric Analysis and Design of Ducted Rotors," 2005

[7] D. H. Shim, Hierarchical Flight Control System Synthesis for Rotorcraft-based Unmanned Aerial Vehicles, *Ph. D. Dissertation*, Department of Engineering-Mechanical Engineering, university of California, Berkeley, 2000.